ELSEVIER

Soil Dynamics and Earthquake Engineering 25 (2005) 547–558

SOIL DYNAMICS AND EARTHQUAKE ENGINEERING

www.elsevier.com/locate/soildyn

Numerical evaluation of slope topography effects on seismic ground motion

George D. Bouckovalas*, Achilleas G. Papadimitriou[1]

Geotechnical Department, School of Civil Engineering, National Technical University, Athens, Greece

Received 15 April 2004; revised 1 October 2004; accepted 11 November 2004

Abstract

This paper presents results of numerical analyses for the seismic response of step-like ground slopes in uniform visco-elastic soil, under vertically propagating SV seismic waves. The aim of the analyses is to explore the effects of slope geometry, predominant excitation frequency and duration, as well as of the dynamic soil properties on seismic ground motion in a parametric manner, and provide qualitative as well as quantitative insight to the phenomenon. Among the main conclusions of this study is that this kind of topography may lead to intense amplification or de-amplification variability at neighboring (within a few tens of meters) points behind the crest of the slope, especially for high frequency excitations. Nevertheless, a general trend of amplification near the crest and de-amplification near the toe of the slope seems to hold for the horizontal motion. As a result of these two findings, it becomes evident that reliable field evidence of slope topography aggravation is extremely difficult to establish. Furthermore, this study highlights the generation of a parasitic vertical component of motion in the vicinity of the slope, due to wave reflections at the slope surface, that under certain preconditions may become as large as the horizontal. Criteria are established for deciding on the importance of topography effects, while approximate relations are provided for the preliminary evaluation of the topographic aggravation of seismic ground motion and the width of the affected zone behind the crest.

Keywords: Earthquakes; Topography effects; Slopes; Numerical analyses; Seismic motion

1. Introduction

The effect of step-like slope topography on seismic ground motion has not been thoroughly examined in the literature, despite that there is indisputable evidence of its significance even from the late 1960s [1]. In fact, this form of surface topography has drawn the least attention among scientists, as compared to hills and canyons, despite its significance in engineering practice. One possible reason is the non-symmetric geometry of step-like slopes, which complicates analytical solutions and favors mostly site-specific numerical simulations whose conclusions are difficult to generalize. Another reason could be the fact that conclusive results from field measurements are difficult to obtain, due to the wave scattering that a step-like slope produces, as discussed later in this paper. As a result, approximate relations and design guidelines are rare in the literature, while relevant provisions have not yet been implemented in most modern seismic codes.

Among the published studies, the majority concerns either specific geometries and seismic excitations [1–6] or examines specific aspects of the phenomenon such as the wave scattering generated at the vicinity of the slope [7] and the effects of a soft soil cap in the area of the slope [8]. The only systematic parametric study found in the literature is that by [9] and [10], which provides valuable insight to the effects of slope inclination i and height H, wave type (P, SH and SV) and wavelength λ, as well as the angle of wave incidence β. Nevertheless, the results of the analyses are presented solely at the crest and at distances equal to H, $2H$ and $4H$ behind it. Furthermore, these studies do not address the effect of two factors that are commonly accounted for in most seismic ground response analyses: the hysteretic

* Corresponding author. Address: 1 Iktinou Street, 15126 Maroussi, Greece. Tel.: +30 210 806 8393; fax: +30 210 772 3428.

E-mail addresses: gbouck@central.ntua.gr (G.D. Bouckovalas), apapad@civil.ntua.gr (A.G. Papadimitriou).

[1] Address: 62 Seferi Street, 15451 N. Psychico, Greece. Tel.: +30 210 675 3326, fax: +30 210 772 3428.

0267-7261/$ - see front matter © 2005 Elsevier Ltd. All rights reserved.
doi:10.1016/j.soildyn.2004.11.008

damping ratio of the soil ξ and the duration of the shaking or the number of equivalent uniform excitation cycles N. Thus, the presented results cannot be readily used for a quantitative assessment of the effect of slope topography on seismic ground motion, in the form of either simple approximate relations or seismic code provisions.

Aiming at this goal, results are presented from an extensive parametric study of step-like slope topography effects, performed with the Finite Difference method [12]. The relevant research was triggered from recent evidence that such effects played an important role in the extent of damage caused by two recent destructive earthquakes in Greece [3,4,11,6]: the 1995 Aigion and the 1999 Athens events. Compared to the study by [9,10], our study is narrower in the sense that it focuses merely on the case of vertically propagating SV waves. On the other hand, it explores in detail the effects of a larger number of problem parameters and provides a continuous assessment of slope topography effects along the ground surface, for a sufficient length behind the crest and in front of the toe of the step-like slope. It should be underlined, that the quantitative assessments hereby provided apply conservatively to SH waves as well, since SH topographic amplification has been shown smaller than that of SV waves [9,10].

2. Methodology outline

The numerical analyses were performed with the Finite Difference method [12], for linear visco-elastic soil with $V_S = 500$ m/s, Poisson's ratio $\nu = 1/3$ and mass density $\rho = 2$ mg/m^3. A schematic illustration of the 2D analyzed mesh and the boundary conditions is provided in Fig. 1. More specifically

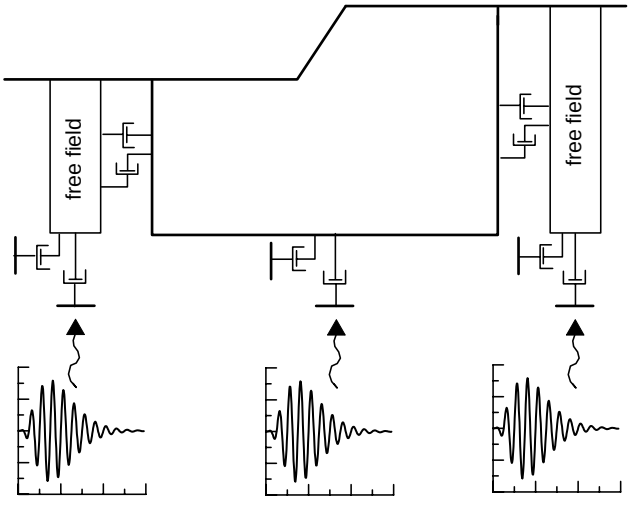

Fig. 1. Schematic illustration of finite difference model for the numerical analyses of step-like slope topography effects.

- 28,000–120,000 quadrilateral zones were used to simulate the uniform soil mass, with a maximum height equal to 1/10–1/20 of the predominant wavelength of the seismic excitation in order to avoid the numerical distortion of its frequency content.
- The width and the height of the mesh were usually set at $20H$ and $5H$, respectively, in order to reduce the effects of artificial wave reflections from the boundaries at the area of interest (near the slope).
- For the same purpose, transmitting boundaries were applied at the base of the mesh, while boundaries simulating the free field were applied at its right and left sides.

Unlike common practice that introduces the seismic excitation at the base of the mesh as a time history of acceleration (or velocity, or displacement), in our analyses a time history of stress was used, in order to avoid artificial wave reflections at the base of the mesh, which are unavoidable in analyses of common practice. Most of the parametric analyses were performed either with a harmonic excitation of 20–40 uniform cycles, or with a Chang's signal excitation aimed to simulate the limited duration as well as the gradual rise and decrease of shaking amplitude (Fig. 1). In addition, a limited number of parametric analyses were performed for actual seismic excitations to explore the effect of a much wider frequency content.

The overall accuracy of the numerical methodology was verified through comparison with analytical solutions for the seismic response of the ground surface across semi-circular shaped canyons, for uniform soil and vertically propagating harmonic SV waves [13]. The choice of this analytical study was dictated by the fact that there are no analytical solutions for step-like slope topography in the reviewed literature and that it is well established and commonly used for calibration of new methods or studies in the literature. A typical comparison between numerical and analytical predictions for the horizontal (U_h) and the (parasitic) vertical (U_v) components of the peak ground surface displacement is shown in Fig. 2, for the particular case of canyon radius $R = 25$ m and wavelength ratio $\lambda/R = 2$.

It is important to notice that the numerical methodology previously outlined does not take consistently into account the effect of soil non-linearity. Namely, shear moduli remain constant (elasticity) and material damping is of the Rayleigh type, i.e. it is frequency dependent and the reference damping of each analysis is the damping value for the frequency of the excitation. For this reason, as well as for the benefit of generalization, the results of the numerical analyses are not evaluated directly, but following normalization against the free-field response of the ground, which is free from any topography effects. For this purpose, each basic 2D analysis was supplemented by two 1D analyses: one for the free field in front of the toe of the slope

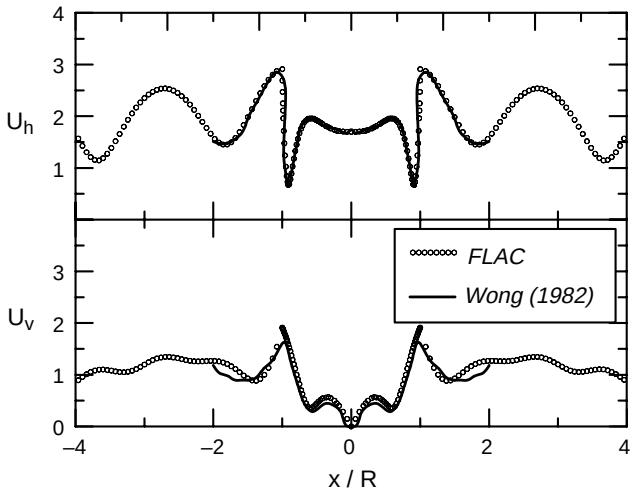

Fig. 2. Analytical verification of numerical scheme for canyon topography (vertical SV wave, $R=25$ m, $\lambda/R=2$).

and the other for the free field behind its crest. This approach is cumbersome, but more accurate than evaluating the free-field response from the results of the 2D analyses alone, at nodes at large distance away from the slope. The reason is that topography effects decrease asymptotically with distance from the slope and may not completely disappear within the analyzed mesh, thus underestimating the overall amplification effects, especially for low intensity motions with small soil damping.

3. Typical results

Typical results from the numerical analyses are presented in Fig. 3, for the specific case of uniform soil, slope inclination $i=30°$, normalized height $H/\lambda=2.0$, critical damping ratio $\xi=5\%$ and six significant cycles of base excitation ($N=6$). This figure shows the variation of the topography aggravation factors $A_h=a_h/a_{h,ff}$ and $A_v=a_v/a_{h,ff}$ with distance from the crest x, where a_h and a_v denote the peak horizontal and peak vertical accelerations at each point of the ground surface.

Parameter $a_{h,ff}$ denotes the free-field value for the peak horizontal acceleration, which is used for normalization of both a_h and a_v, since $a_{v,ff}=0$ for a vertically propagating SV wave in a uniform horizontal soil. Review and interpretation of this figure alone may provide insight to the mechanisms, which control topography effects and may lead to some first conclusions of practical interest. Namely:

(a) Even a purely horizontal excitation, as a vertically propagating SV wave, results in considerable (parasitic) vertical motion at the ground surface near the slope. This component of ground motion is independent of any vertical excitation induced to the base of the slope by the earthquake itself and, consequently, it has to be superimposed to it. The results of the parametric analyses show that the vertical (parasitic) component of seismic motion may become comparable to the horizontal free-field motion.

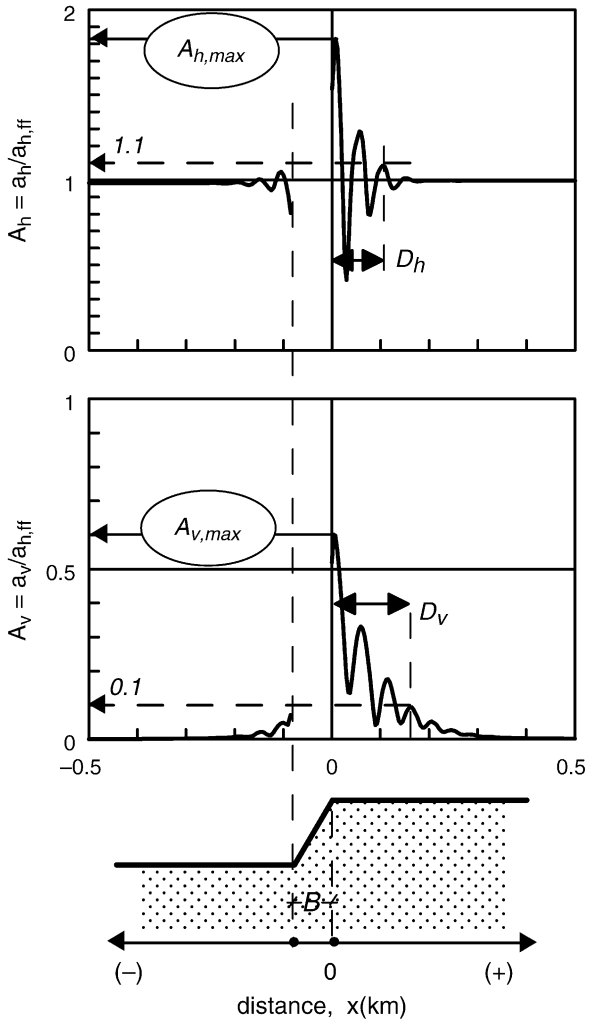

Fig. 3. Typical results for the topographic amplification of the peak horizontal A_h and the parasitic vertical A_v acceleration, as a function of horizontal distance x from the crest (results for $H/\lambda=2$, $i=30°$, $N=6$, $\xi=5\%$).

(b) The topography aggravation of the horizontal ground motion, expressed through the peak acceleration ratio $A_h=a_h/a_{h,ff}$, fluctuates intensely with distance away from the crest of the slope, alternating between amplification ($A_h>1.0$) and de-amplification ($A_h<1.0$) within very short horizontal lengths. For the typical results of Fig. 3, this length is approximately 25 m, i.e. equal to $H/2$ (or equal to λ for this case of $H/\lambda=2$). Similarly, the topographic apparition of parasitic vertical motion expressed via A_v is also intensely variable with distance. The local maxima and minima of A_v occur again at distances equal to $H/2$, but their locations do not necessarily coincide with the respective points for the A_h. These findings regarding the fluctuation of topographic aggravation imply that its

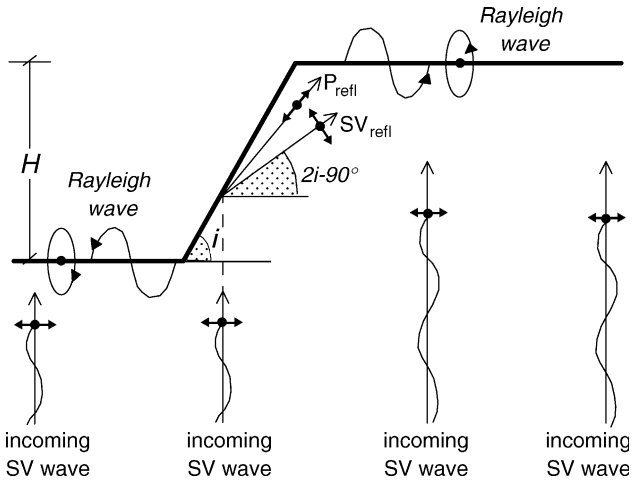

Fig. 4. Schematic illustration of incoming SV waves and induced P_{refl}, SV_{refl} and Rayleigh in the case of step-like slopes ($i \geq 45°$).

experimental verification through inverse analysis of structural damage is very crude, and that actual ground motion recordings near slopes must be obtained via very dense seismic arrays.

(c) It is also worth noticing that the horizontal ground motion is de-amplified at the toe of the slope and amplified near the crest. As a result, topography aggravation may be seriously overestimated, when calculated as the peak seismic ground motion at the crest over that at the toe of the slope. For example, for the results of Fig. 3, this procedure would give $A_h \cong 1.70/0.80 = 2.13$, which is higher than the peak topography aggravation behind the crest $A_{h,max} = 1.83$. This overestimation may reach 100% for steeper slopes (Fig. 5) and may explain, at least in part, why field measurements (without appropriate free field selection) of topography aggravation are usually significantly higher than analytical predictions [14].

Findings (a) and (b) above can be readily attributed to the reflection of the incoming SV waves on the inclined free surface of the slope (Fig. 4), which leads to reflected P and SV waves impinging obliquely at the free ground surface behind the crest, as well as Rayleigh waves. All these induced waves have a strong vertical component. In addition, they arrive with a time lag and a phase difference at the different points of the ground surface so that their superposition to the incoming SV waves may lead either to amplification or to de-amplification of the horizontal seismic motion.

4. Approximate relations

In all, 90 parametric analyses were performed in order to assess the effect of the following potentially important parameters (Tables 1 and 2):

Table 1
Pairs of normalized height H/λ and slope angle i for the parametric analyses of step-like slopes with small soil damping ($\xi \leq 5\%$), under harmonic base excitation

i (°)	H/λ									
	0.05	0.10	0.15	0.20	0.30	0.45	0.70	1.00	1.30	2.00
10		X		X		X		X		
20		X		X		X		X		
30	X	X	X	X	X	X	X	X	X	X
45	X	X	X	X	X	X	X	X	X	X
60	X	X	X	X	X	X	X	X	X	X
75		X		X		X		X		
90		X		X		X		X		

- the slope inclination i(deg) or $I = i/90$,
- the normalized height of the slope H/λ, where λ denotes the predominant wave length of the incoming SV waves,
- the number of significant excitation cycles N, defined for a stress level equal to the 1/2 of the peak,
- the critical hysteretic damping ratio ξ of the soil.

Note that the 90 parametric analyses were performed for base excitations with a predominant period T_e ranging from 0.05 to 2.0 s, a range practically covering the large majority of possible earthquake events. This range of T_e is what produces the range of $H/\lambda = 0.05$–2.0 shown in Tables 1 and 2, since all analyses were performed for a slope of height $H = 50$ m and uniform $V_S = 500$ m/s. Nevertheless, topographic aggravation results coincide for step-like slopes with different values of H and λ but the same value of H/λ, a fact that allows for the generalization of the presented results for a very large range of soil and excitation conditions.

Figs. 5–8 present selected results from the parametric analyses demonstrating the effects of slope angle i, normalized height H/λ, number of significant excitation cycles N and soil damping ξ. In broad terms, it is observed that the slope angle i and the normalized height of the slope H/λ have a significant and non-univocal effect on the aggravation of the horizontal and vertical ground motions (factors A_h and A_v), as well as on the distance to the free field in front and behind the slope (Figs. 5 and 6). On the contrary, Figs. 7 and 8 show that the hysteretic damping ratio of the soil ξ has a significant effect only on the distance

Table 2
Pairs of significant excitation cycles N and soil damping ξ for the parametric analyses of step-like slopes with $H/\lambda = 2.0$ and $i = 30°$ (X) or $H/\lambda = 0.20$ and $i = 75°$ (O), under Chang's signal base excitation

ξ (%)	N						
	1	2	3	4	6	8	12
0	X	X, O	X	X	X, O	X	X, O
2	X	X	X	X	X	X	X
5	X	X	X	X	X	X	X
10	X	X, O	X	X	X, O	X	X, O
20	X	X, O	X	X	X, O	X	X, O

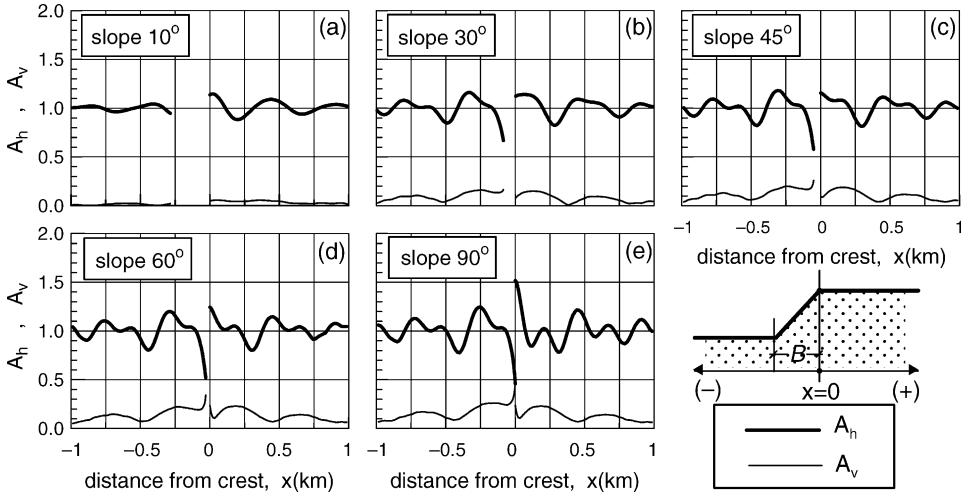

Fig. 5. Effect of slope inclination i on the amplification of peak horizontal A_h and apparition of parasitic vertical A_v acceleration, as a function of horizontal distance x from the crest of a step-like slope ($H/\lambda=0.2$, harmonic motion, $\xi<5\%$).

to the free field, while the number of significant excitation cycles N has a relatively minor overall effect. Practically speaking, our results in terms of A_h and A_v from analyses for small soil damping ($\leq 5\%$) agree in both qualitative and quantitative terms with the work of [9,10]. As an example, Fig. 9 compares our results in terms of A_h and A_v at the crest of step-like slopes (symbols) with the respective results (lines) from [10] and shows that the two distinctly different methodologies of analyses (Finite Difference method here versus generalized consistent transmitting boundary method in [9,10]) produce practically identical results.

Furthermore, in order to increase the applicability of the results of the parametric analyses, a database was created tabulating the most important input variables and output parameters of all analyses. Namely, the input of each analysis was introduced in terms of variables $I(=i/90)$, H/λ, N and ξ. The selection of the output parameters was less straightforward. Addressing this issue from an engineering point of view, of interest for design purposes are the peak values of the topography aggravation factors $A_{h,max}$ and $A_{v,max}$ behind the crest, in the horizontal and vertical direction, respectively (Fig. 3). Moreover, of practical importance is also the distance behind the crest for which topography aggravation is significant, defined separately for the horizontal and for the vertical directions and denoted by D_h and D_v, respectively. Note that, from an engineering point of view, it was assumed that free field conditions apply at distances D_h and D_v behind the crest where $A_h \leq 1.10$ and $A_v \leq 0.10$, respectively (Fig. 3).

Hence, four (4) output parameters were tabulated in the database, which were sequentially related to the four (4) input variables via the following general expressions:

$$A_{h,max} = 1 + F_{Ah}\left(\frac{H}{\lambda}\right) G_{Ah}(I) H_{Ah}(\xi) J_{Ah}(N) \quad (1)$$

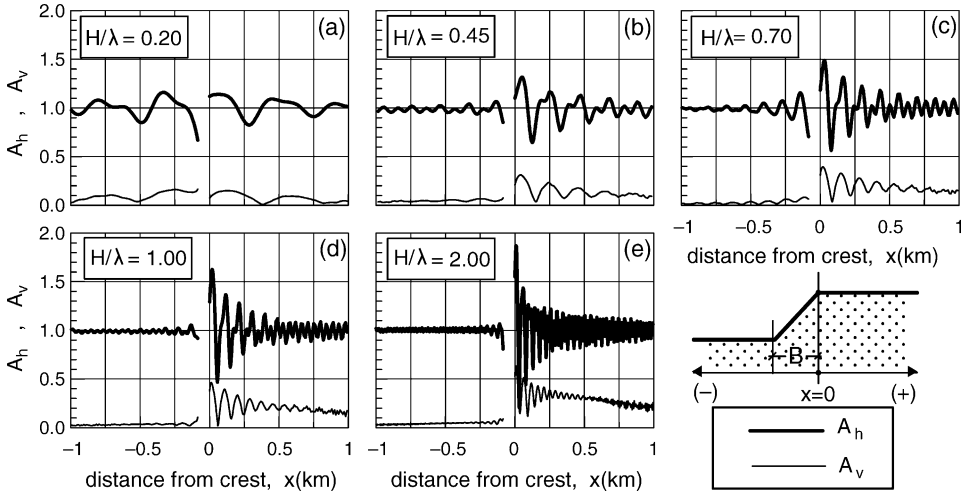

Fig. 6. Effect of normalized height H/λ on the amplification of peak horizontal A_h and apparition of parasitic vertical A_v acceleration, as a function of horizontal distance x from the crest of a step-like slope ($i=30°$, harmonic motion, $\xi<5\%$).

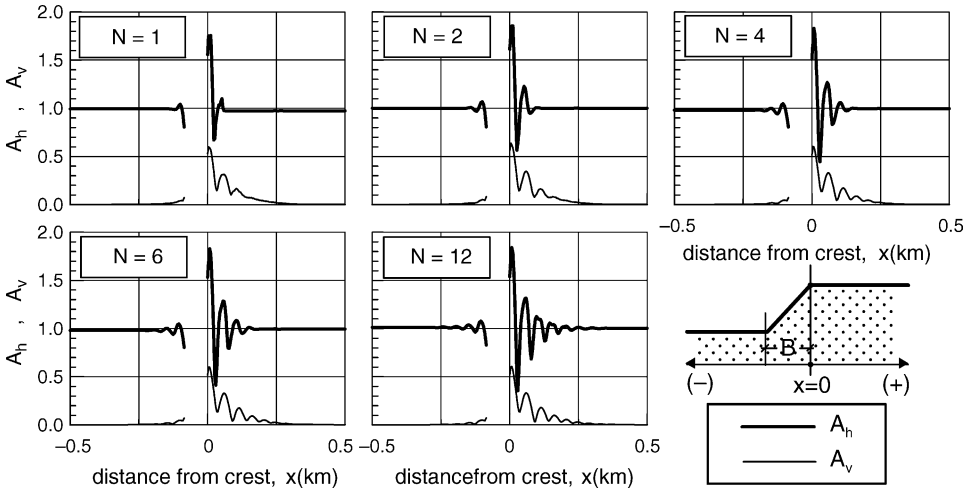

Fig. 7. Effect of number of significant cycles N on the amplification of peak horizontal A_h and apparition of parasitic vertical A_v acceleration, as a function of horizontal distance x from the crest of a step-like slope ($H/\lambda=2$, $i=30°$, $\xi=5\%$).

$$A_{v,max} = F_{Av}\left(\frac{H}{\lambda}\right) G_{Av}(I) H_{Av}(\xi) J_{Av}(N) \quad (2)$$

$$D_h/H = F_{Dh}\left(\frac{H}{\lambda}\right) G_{Dh}(I) H_{Dh}(\xi) J_{Dh}(N) \quad (3)$$

$$D_v/H = F_{Dv}\left(\frac{H}{\lambda}\right) G_{Dv}(I) H_{Dv}(\xi) J_{Dv}(N) \quad (4)$$

The final form of functions F, G, H and J in Eq. (1)–(4) are analytically defined in Table 3 and shown graphically in

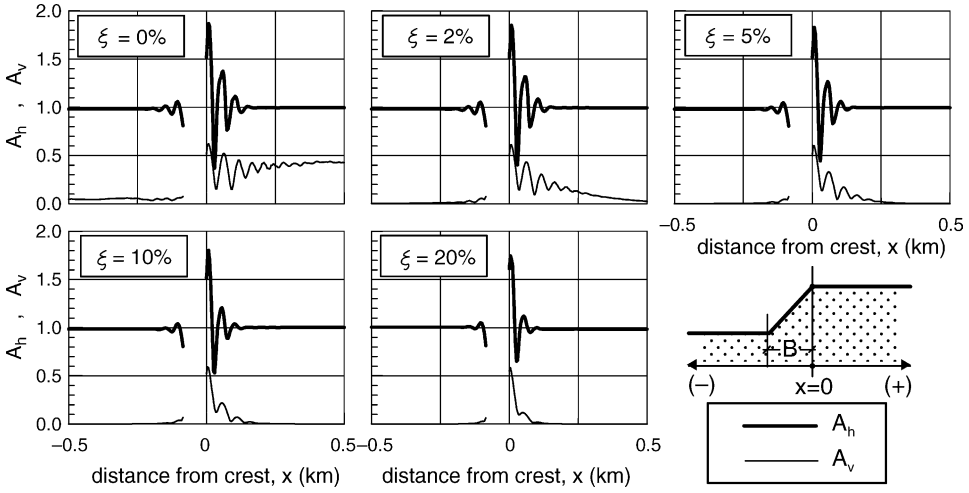

Fig. 8. Effect of soil damping ξ on the amplification of peak horizontal A_h and apparition of parasitic vertical A_v acceleration, as a function of distance x from the crest of a step-like slope ($H/\lambda=2$, $i=30°$, $N=4$).

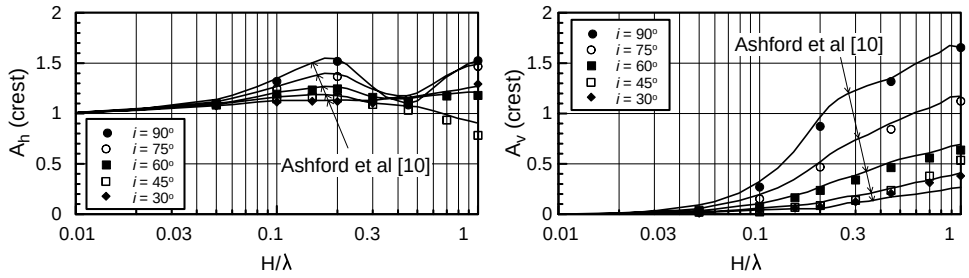

Fig. 9. Comparison of results from parametric analyses with published predictions for the crest of step-like uniform slopes ($\xi<5\%$, harmonic base excitation).

Table 3
Analytical form of functions F, G, H and J in the proposed approximate relations for topography aggravation (Eqs. (1)–(4))

Parameter	$F(H/\lambda)$	$G(I)$	$H(\xi)$	$J(N)$
$A_{h,max}$	$(H/\lambda)^{0.4}$	$(I^2+2I^6)/(I^3+0.02)$	$1/(1+0.9\xi)$	0.225
$A_{v,max}$	$(H/\lambda)^{0.8}$	$I^{0.5}+1.5I^5$	$1/(1+0.15\xi^{0.5})$	0.75
D_h/H	$(H/\lambda)/((H/\lambda)^2+0.2)$	$(I^{1.5}+3.3I^8)/(I^4+0.07)$	$1/(0.71+3.33\xi)$	$N^{0.43}$
D_v/H	$(H/\lambda)/((H/\lambda)^2+0.2)$	$(I^{1.5}+3.3I^8)/(I^4+0.07)$	$0.233/\xi^{0.78}$	1.00

Fig. 10. Note that for better accuracy, the statistical analysis that produced the form of functions F, G, H and J was performed in two steps. First, the effect of each (practically independent) variable was explored separately, by selecting cases for which the values of the remaining variables varied within a narrow range, so that the general form of functions F, G, H and J could be identified. The quantitative expression of the proposed relations was consequently established from a multivariable regression analysis of the entire database, according to the Newton–Raphson iterative procedure.

The comparison between approximate and numerical predictions of $A_{h,max}$, $A_{v,max}$, D_h/H and D_v/H is shown in the four plots of Fig. 11. In these plots, each symbol corresponds to a different analysis and is obtained, on one hand, using as coordinates the value of the parameter from the numerical analysis, and, on the other hand, the respective value from the approximate relation. The diagonal lines in each plot correspond to perfect match between the compared values, while the shaded area provides an estimate of the anticipated relative difference. Observe that, the symbols are equally scattered on both sides of the diagonal lines and that the standard deviation of the relative error of the approximate relations ranges from 29 to 40%, depending on the parameter at hand.

Elaborating on the proposed approximate relations, it is deduced that for common conditions of practical interest (i.e. $H/\lambda=0.2$–1.0, $i=25$–75° and $\xi=5$–15%):

(a) The range of computed values for the peak horizontal and vertical aggravation factors behind the crest are $A_{h,max}=1.20$–1.50 and $A_{v,max}=0.10$–1.10, while
(b) The distance to the free field D_{ff}, set as the maximum of D_h and D_v, is equal to (2–8)H.

Comparing these results to what code provisions prescribe provides useful conclusions on the overall compatibility of the latter with theory-based predictions. It was found that merely the European EC-8 (2000 and draft 2002) and the French seismic codes PS-92 [15] contain provisions for topographic amplification factors. Specifically, the foregoing range of $A_{h,max}$ is broadly comparable to the provisions of the European EC-8 (2000 and draft 2002) and the French PS-92 seismic codes, which prescribe 20 and 40% increase of the peak horizontal acceleration at the most. However, both codes totally overlook the generation of a parasitic vertical motion component. Furthermore, the distance to the free field estimated in this study is significantly larger than that mentioned in the codes. Namely, the EC-8 (2000 and draft 2002) requires vaguely that peak horizontal accelerations are increased 'near the top edge' of slopes, while the explicit evaluation of the distance to the free field provided by PS-92 does not exceed the height of the slope H. These code-prescribed distances to free field are considered very short, even if the limits of the topography

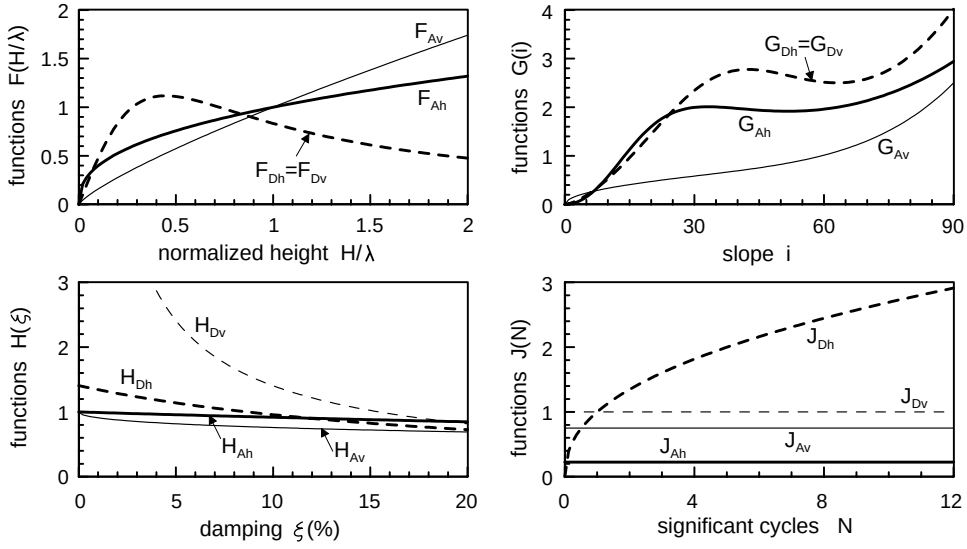

Fig. 10. Form of functions $F(H/\lambda)$, $G(i)$, $H(\xi)$ and $J(N)$ entering the approximate relations for the estimation of parameters $A_{h,max}$, $A_{v,max}$, D_h/H and D_v/H.

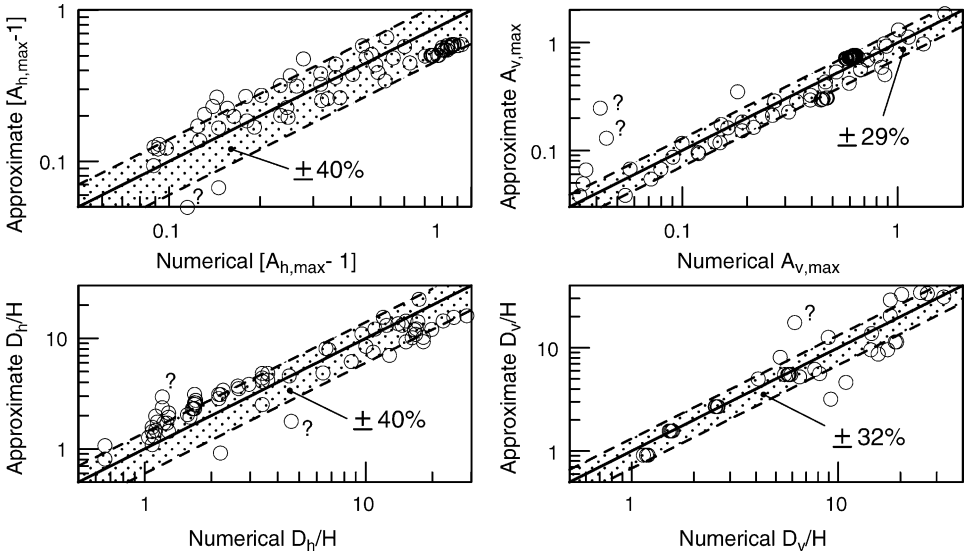

Fig. 11. Comparison of $A_{h,max}$, $A_{v,max}$, D_h/H and D_v/H estimates from approximate relations and numerical analyses for all the cases in the database.

aggravation factors for the free field are increased to $A_h \leq 1.20$ and $A_v \leq 0.20$.

Equally valuable conclusions may be drawn with regard to the criteria for considering topography aggravation in practice. For this purpose, Fig. 12 shows the contours for $A_{h,max} = 1.10$ and 1.20 and $A_{v,max} = 0.10$ and 0.20 in terms of the two main variables, H/λ and $I = i/90$. The third variable that appears in the respective relations, i.e. soil damping ξ, has a relatively minor effect on $A_{h,max}$ and $A_{v,max}$ and it is consequently fixed to an average value of 10%. Comparing the two sets of contours, it becomes evident that the criteria for significant topography aggravation of the horizontal seismic motion (i.e. $A_{h,max} \geq 1.10$ and 1.20) are stricter than those for the appearance of a significant parasitic vertical seismic motion (i.e. $A_{v,max} = 0.10$ and 0.20). Thus, in a simplified manner, one may focus upon the former, and require that:

- H/λ 0.03 and $i > 10°$ for at least 10% topographic aggravation of the horizontal ground motion, and
- $H/\lambda > 0.16$ and $i > 17°$ for at least 20% topographic aggravation of the horizontal ground motion.

It is noteworthy that the French (PS-92 [15]) and the European (EC-8) seismic codes provide similar lower limits for topography effects on seismic ground motion, with the difference that the criteria for slope height H are given in nominal rather than in normalized values. More specifically, the PS-92 requires that $H > 10$ m and $i > 22°$, while the EC-8 requires that $H > 30$ m and $i > 15°$. For natural slopes in stiff soil or soft rock formations (with shear wave velocity $V_S >$ 400 m/s), and common seismic excitations with predominant period larger than about 0.20 s, the foregoing lower code limits are in broad agreement with the hereby proposed limits for 20% topography aggravation which lead to $H >$ 13 m and $i > 17°$.

5. Comparison with site-specific numerical studies

The excitations used to perform the parametric analyses were harmonic or nearly harmonic, with a very narrow frequency spectrum as compared to actual seismic excitations. To explore the importance of this limitation on

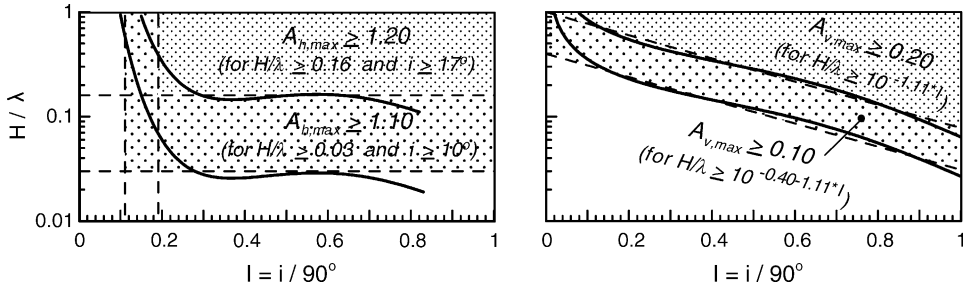

Fig. 12. Lower limits of normalized slope height H/λ and slope angle i, for which topography effects become significant.

the accuracy of the proposed relations, they have been applied to predict the results of four numerical case studies, performed for actual seismic excitations. Three of the case studies were performed independently of the present study, using the equivalent linear Finite Element method, for the evaluation of topography effects anticipated during the Aigion (June 15, 1995) and the Athens (September 7, 1999) earthquakes in Greece. It is noted that in all above cases there were no simultaneous seismic recordings behind the crest and at free field that could be used to verify directly the respective site-specific numerical analyses. Hence, their accuracy is assessed only indirectly, on the basis of the increased structural damage intensity in the vicinity of the crest. The fourth case study was part of the present effort and aimed at providing a more extensive comparison between approximate and numerical predictions.

5.1. Aigion city, during the Aigion earthquake (June 15th 1995)

According to [4], the topography at the northern part of Aigio (overlooking the harbor) creates a slope of angle $i \cong 45°$ and height $H \cong 80$ m (Fig. 13(a), section a–a), while the earthquake had a predominant period $T_e = 0.4$–0.5 s. The shear wave velocity V_S increases gradually with depth, without providing for a sharp contrast at a specific depth that would imply the existence of seismic bedrock. Hence, the average V_S varies between 400 and 1000 m/s, which corresponds to a predominant wavelength $\lambda = 160$–500 m. The acceleration time history (recorded at OTE site, Fig.13(a)) had few significant cycles ($N = 2$–3), while damping ξ must have ranged between 5 and 10%.

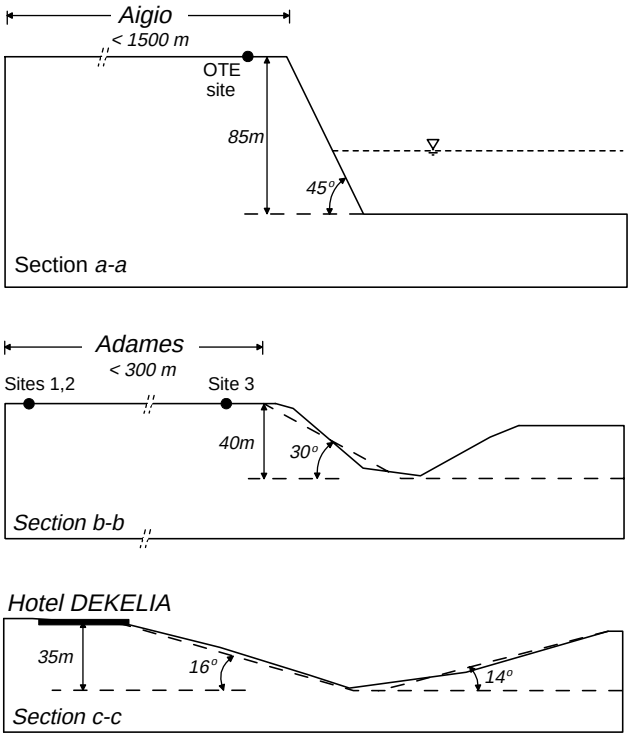

Fig. 13. Topography at three sites in Greece where the increased structural damage behind the crest observed during strong recent earthquakes has been investigated with site-specific 2D numerical analyses.

Based on the case-specific analyses of [4], the maximum amplification of the horizontal acceleration behind the crest is of the order of 1.40, while the distance to free field behind the crest is approximately 500 m (i.e. 6.2 H). Based on the approximate relations proposed here, for a range of $H/\lambda = 0.16$–0.50 it is deduced that $A_{h,max} = 1.2$–1.32, while $D_h/H = 3.5$–5.6.

5.2. Adames area, during the Athens earthquake (September 7th 1999)

According to [6], the topography at the Adames area (overlooking the Kifissos river) creates a slope of angle $i \cong 30°$ and height $H \cong 40$ m (Fig. 13(b), section b–b), while the average shear wave velocity V_S ranges between 350 and 600 m/s, without a sharp contrast at a specific depth implying the existence of seismic bedrock. There were no seismic recordings at the area of interest, but recordings at other locations show that the motion must have had higher predominant frequency than the Aigio earthquake, namely a predominant period $T_e = 0.10$–0.20 s. Hence, the predominant wavelength in the area must have ranged between $\lambda = 35$–120 m. Again, on the basis of the recordings at other locations, the time-history must have had few cycles ($N = 2$–4), while damping ξ must have ranged between 5 and 10%.

Based on the site-specific numerical results described by [6], the peak amplification ratio of the horizontal ground acceleration is of the order of 1.3–1.5, while the respective distance to free field is approximately equal to 75–100 m or, i.e. $1.9H$–$2.5H$. The same researchers provided estimates of the peak parasitic vertical acceleration behind the crest equal to 0.24–0.26 of the horizontal acceleration at free field. Based on the approximate relations proposed here, for a range of $H/\lambda = 0.33$–1.14 it is deduced that $A_{h,max} = 1.28$–1.45, $A_{v,max} = 0.17$–0.47, while $D_h/H = 2.7$–4.6.

5.3. Area of Hotel 'Dekelia', during the Athens earthquake (September 7th 1999)

According to [3], the topography at the Hotel 'Dekelia' is a mild slope overlooking the Kifissos river, with slope angle $i \cong 16°$ and height $H \cong 35$ m (Fig. 13(c), section c–c), while the average shear wave velocity V_S ranges between 400 and 600 m/s, without a clear presence of seismic bedrock. As in the previous case, the excitation period is $T_e = 0.1$–0.2 s providing for predominant wavelengths in the range of $\lambda = 40$–120 m, while the main shock must have had few significant cycles ($N = 2$–4), and damping ξ must have ranged between 5 and 10%.

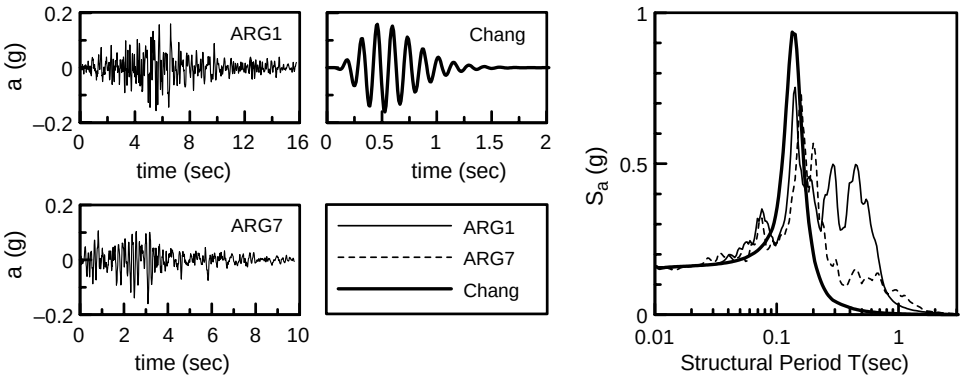

Fig. 14. Acceleration time-histories and elastic response spectra of two earthquake records and an equivalent Chang's signal-type excitation with respect to amplitude, number of significant cycles and predominant period.

Based on the results of the site-specific analyses described by [3], the amplification ratio of the horizontal ground acceleration at the location of the hotel ranged between 0.75 and 1.35 for various excitations, with the largest values being the most probable since they correspond to the high-frequency motions. Similarly, the distance to free field should not have exceeded 70–100 m (i.e. $D_h/H=2$–3). No data are reported for the parasitic vertical component of seismic ground motion. According to the approximate relations proposed herein, for the range of normalized slope heights $H/\lambda=0.30$–0.88, it is expected that $A_{h,max}=1.16$–1.25 and $D_h/H=1.5$–2.

5.4. Frequency dependence of topography aggravation

The last numerical case study concerned a step-like slope with $H=50$ m and $i=60°$, cut within a uniform visco-elastic medium with $V_S=500$ m/s, $\xi=2\%$, Poisson's ratio $\nu=1/3$ and mass density $\rho=2$ Mg/m^3. Three different seismic excitations were used: two actual seismic records (ARG1 and ARG7), with similar predominant periods $T_e=0.14$–0.16 s and number of significant cycles $N=2$–4.5, and a Chang's signal with similar characteristics. All excitations were scaled to the same peak ground acceleration of 0.16 g. The time histories and the 5% damped elastic response spectra of these base excitations are summarized in Fig. 14.

The results of the numerical analyses are compared in Figs. 15 and 16. More specifically, Fig. 15 compares the topographic aggravation of the peak horizontal A_h and vertical accelerations A_v as a function of the horizontal distance in front and behind the crest. Furthermore, Fig. 16 compares the topographic aggravation of the normalized horizontal spectral accelerations $S_a^*=S_a/a_h$ at two locations of significant importance: (a) the crest of the slope and (b) the point behind the crest where the peak aggravation of horizontal acceleration is observed. Note that Fig. 16(b) disregards the fact that the points of peak horizontal aggravation behind the crest for the three different excitations do not coincide. Nevertheless, the presented comparison is justified given the geographic proximity of the three points and the fact that the frequency content of the motion at the locations of peak aggravation is of significant engineering interest. Overall, the comparisons in Figs. 15 and 16 show that all three analyses provide compatible results, with the Chang's signal excitation leading to rather conservative estimates of the topographic aggravation of the peak ground and the spectral accelerations. Furthermore, these comparisons imply that topography mostly affects the peak ground acceleration and seems to alter the frequency content of the ground motion to a lesser degree. The width of the affected zone behind the crest is under-predicted for

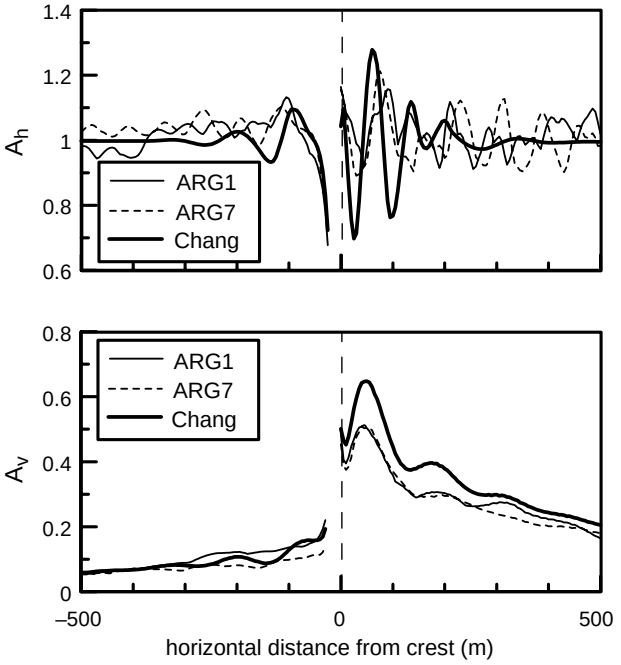

Fig. 15. Topographic amplification of horizontal acceleration A_h and apparition of vertical parasitic acceleration A_v as a function of horizontal distance from the crest of a step-like slope, for the two realistic earthquake motions and the Chang's signal-type excitation of Fig. 14.

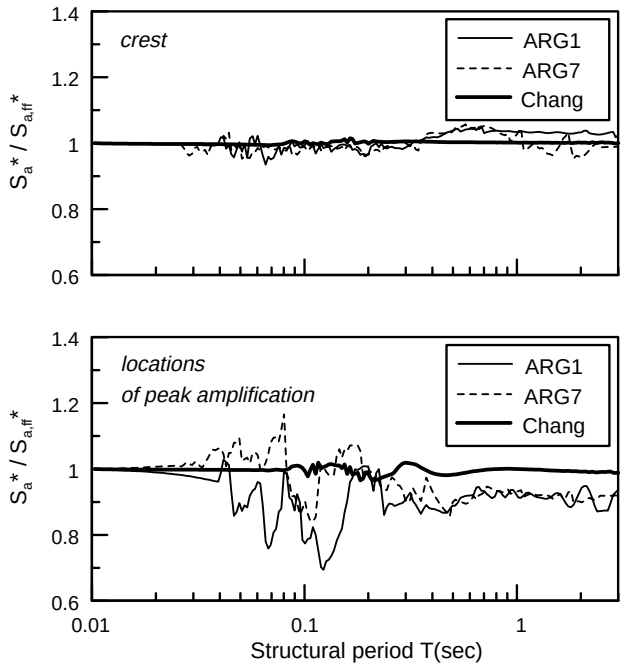

Fig. 16. Topographic amplification of normalized spectral horizontal amplification S_a^* at the crest and the locations of peak ground amplification of a step-like slope, for the two realistic earthquake motions and the Chang's signal-type excitation of Fig. 14.

the horizontal component of motion and over-predicted for the vertical. However, it is reasonable to expect that these differences may be reduced for more realistic, higher ξ values.

6. Conclusions

The main findings that have emerged from this numerical study of topography effects for step-like slopes are the following:

(a) The effect of slope topography is to alter (amplify or de-amplify) the peak horizontal seismic ground acceleration in front and behind the crest and also to produce a parasitic vertical acceleration that has to be superimposed to that of the incoming seismic excitation. Topography effects fluctuate intensely with distance away from the slope, so that detecting them on the basis of field measurements alone requires a dense seismic array.

(b) Topography effects become important for normalized height ratios $H/\lambda > 0.16$ and slope inclinations $i > 17°$. If these conditions are met, the peak values of topography aggravation factors for the horizontal and the vertical ground acceleration behind the crest usually vary between $A_{h,max} = 1.20–1.50$ and $A_{v,max} = 0.10–1.10$, while free field conditions behind the crest are usually met at a distance $D_{ff} = (2–8)H$.

(c) The few seismic codes that deal with slope topography aggravation of seismic motion (EC-8 and PS-92) are reasonable with regard to the maximum increase of peak horizontal accelerations. Nevertheless, they neglect the generation of parasitic vertical acceleration and seriously underestimate the distance from the slope where topography effects become negligible.

In addition, this paper proposes a set of approximate relations for the preliminary evaluation of topography aggravation factors, based on a statistical study of results from 90 parametric analyses of step-like slopes. These relations provide reasonable predictions, as compared to the parametric analyses (standard deviation of the error ranging from 29 to 40%) as well as to detailed numerical analyses for actual seismic excitations and soil profiles. Note that the proposed relations should only be used for soil and excitation conditions similar to those of the parametric analyses on which they were based. In this sense, and given the H/λ normalization, the only restriction for their use is that the investigated step-like slope has either a practically constant or a smoothly increasing dynamic stiffness with depth, without any intense stiffness contrast implying a soil–bedrock interface.

It is acknowledged that the lack of experimental evidence for comparison and calibration of the findings of this numerical study is a serious obstacle in generalizing its results with the goal of providing a theoretically consistent set of code provisions. However, this is a problem for any numerical study on topography effects, since an experimental verification faces the objective difficulty of intense spatial variability of topographic aggravation depicted in this study. Hence, future field studies are worth focusing on the experimental verification of this phenomenon with dense recording arrays deployed at carefully selected sites with well-established geotechnical properties at various locations and depths.

Acknowledgements

The research reported herein has been funded by the Earthquake Protection and Planning Organization of Greece (ΟΑΣΠ). In addition, fellow Civil Engineers Evangelos Drandakis, Theodoros Vourvahakis, Stefanos Vasdekis and Ioulia Sofianou participated in the execution of the parametric analyses. These valuable contributions are gratefully acknowledged.

References

[1] Idriss I, Seed HB. Response of earthbanks during earthquakes. J Soil Mech Found Div ASCE 1967;93(SM3):61–82.

[2] Idriss I. Finite element analysis for the seismic response of earth banks. J Soil Mech Found Div ASCE 1968;94(SM3):617–36.

[3] Athanasopoulos GA, Pelekis PC, Xenaki VC. Topography effects in the Athens 1999 earthquake: the case of hotel Dekelia. Proceedings of fourth international conference on recent advances in geotechnical earthquake engineering and soil dynamics, San Diego, March (in CD-ROM) 2001.

[4] Bouckovalas GD, Gazetas G, Papadimitriou AG. Geotechnical aspects of the Aegion (Greece) earthquake. Proceedings of second international conference on geotechnical earthquake engineering, Lisbon, June. vol. 2 1999 p. 739–48.

[5] Castellani A, Peano L. Seismic response of topographic irregularities. Proceedings of third international earthquake microzonation conference, Seattle. vol. II 1982 p. 533–40.

[6] Gazetas G, Kallou PV, Psarropoulos PN. Topography and soil effects in the Ms = 5.9 Parnitha Athens earthquake: the case of Adames. Nat Hazards 2002;27:133–69.

[7] Boore DM, Harmsen SC, Harding ST. Wave scattering from a step change in surface topography. Bull Seismol Soc Am 1981;71(1):117–25.

[8] Ohtsuki A, Harumi K. Effect of topography and subsurface inhomogeneities on seismic SV waves. Earthquake Eng Struct Dyn 1983;11:441–62.

[9] Ashford S, Sitar N. Analysis of topographic amplification of inclined shear waves in a steep coastal bluff. Bull Seismol Soc Am 1997;87(3): 692–700.

[10] Ashford S, Sitar N, Lysmer J, Deng N. Topographic effects on the seismic response of steep slopes. Bull Seismol Soc Am 1997;87(3): 701–9.

[11] Bouckovalas GD, Kouretzis GK. A review of soil and topography effects in Athens 09/07/199 (Greece) earthquake. Proceedings of fourth international conference on recent advances in geotechnical earthquake engineering and soil dynamics, San Diego, March (in CD-ROM) 2001.

[12] Itasca Consulting Group, Inc. FLAC: fast lagrangian analysis of continua. User's manual; 1993.

[13] Wong HL. Effect of surface topography on the diffraction of P, SV and Rayleigh waves. Bull Seismol Soc Am 1982;72(4):1167–83.

[14] Geli L, Bard PY, Jullien B. The effect of topography on earthquake ground motion: a review and new results. Bull Seismol Soc Am 1988; 78(1):42–63.

[15] PS-92. Règles de construction parasismique: Règles PS applicables aux bâtiments. Normes NF P 06-013, Troisième Tirage; 1999.